## Unexpected Rise in Nuclear Collectivity from Short-Range Physics

Kevin S. Becker, <sup>1</sup> Kristina D. Launey, <sup>1</sup> Andreas Ekström, <sup>2</sup> Tomáš Dytrych, <sup>1,3</sup> Daniel Langr, <sup>4</sup> Grigor H. Sargsyan, <sup>5</sup> and Jerry P. Draayer <sup>1</sup>

Department of Physics and Astronomy, Louisiana State University, Baton Rouge, LA 70803, USA
Department of Physics, Chalmers Institute of Technology, Gothenburg, Sweden
Nuclear Physics Institute of the Czech Academy of Sciences, 250 68 Řež, Czech Republic
Department of Computer Systems, Faculty of Information Technology,
Czech Technical University in Prague, Prague 16000, Czech Republic
Facility for Rare Isotope Beams, Michigan State University, East Lansing, MI 48824, USA
(Dated: January 3, 2025)

We discover a surprising relation between the collective motion of nucleons within atomic nuclei, traditionally understood to be driven by long-range correlations, and short-range nucleon-nucleon interactions. Specifically, we find that quadrupole collectivity in low-lying states of <sup>6</sup>Li and <sup>12</sup>C, calculated with state-of-the-art *ab initio* techniques, is significantly influenced by two opposing S-wave contact couplings that subtly alter the surface oscillations of one largely deformed nuclear shape, without changing that shape's overall contribution within the nucleus. The results offer new insights into the nature of emergent nuclear collectivity and its link to the underlying nucleon-nucleon interaction at short distances.

While the emergence of collective phenomena in atomic nuclei from elementary particle considerations has been recently shown in large-scale ab initio calculations [1], how exactly the underlying physics of quarks and gluons imparts collectivity remains elusive. Nuclear collectivity is historically understood to be driven by longrange correlations that deform the nucleus; deformed nuclei can rotate, which involves all particles in the system in a correlated motion [2]. Every nucleus can take on several shapes, typically one or two [1], and the deformation of each nuclear shape is often inferred from its equilibrium "static" deformation, whereas the "snapshots" of the shape's surface dynamics are called dynamical deformation (Fig. 1). The extent of collectivity is informed by electric quadrupole moments  $Q_2$ , or equally, reduced transition strengths B(E2), which increase with larger deformation [3]. The prevalence of large deformation in most nuclei, even those with practically spherical ground states where shapes of different deformation coexist [4], is now evident from the vast body of experimental data [5–13]. Furthermore, recent measurements of B(E2) strengths have achieved such precision that they can now test microscopic approaches and the underlying inter-nucleon forces they adopt (see, e.g., [14, 15]).

Yet, with no available nuclear force expressed directly in quark and gluon degrees of freedom, it remains unclear which parts of such fundamental interactions are responsible for the universal preference of large deformation, and are capable of substantially influencing collectivity. Fortunately, some insight emerges when the nuclear force is modeled with the state-of-the-art chiral effective field theory (EFT) (see, e.g., [16–19]). In particular, chiral EFT starts from nucleon and pion degrees of freedom, while accounting for the symmetry and symmetry-breaking patterns of the underlying theory of quantum chromodynamics (QCD). Chiral EFT hence provides a link to quark-gluon physics, which at low energies relevant to nuclei is averaged and encapsulated in

its so-called low energy constants (LECs). The nuclear force thus partly depends on these unknown parameters which are typically fit to experimental few-nucleon data and might eventually be informed by QCD [20–22]. In this framework, we can directly probe the sensitivity of collective observables to the physics at very short distances (high energies) by studying the subset of LECs that determine the nucleon-nucleon (NN) contact interaction strengths.

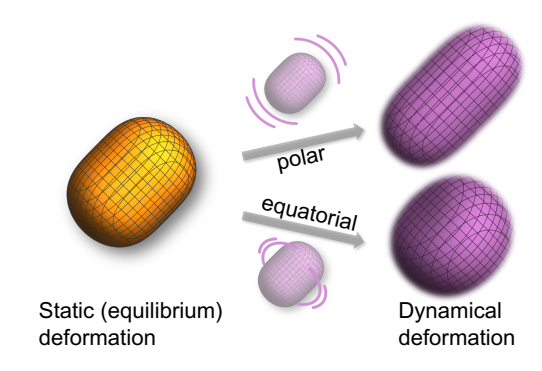


FIG. 1: Schematic illustration, based on large-scale *ab initio* calculations [1], of the static deformation (yellow) of a nuclear shape and two snapshots of its dynamical deformation (purple) arising from surface oscillations (particle-hole excitations): "polar" aligned with the symmetry axis, and "equatorial" in the orthogonal plane.

In this letter, we report on a surprising new result: that nuclear collectivity can be enhanced not only through the traditional mechanism of shapes with ever-larger deformation, but also by a spatial redistribution of the surface oscillations of nuclear shapes that is mediated by the short-range S-wave NN contact interaction. Specifically, we discover that the LEC-independent forces, which include intermediate- and long-range interactions, determine the nuclear shapes and their contributions within a state, while at the same time variations of the short-range

contact forces can further increase or decrease collectivity. The unexpected origin of this interesting effect, we find here, is subtle changes in the surface oscillations of one largely deformed and predominant shape.

We examine this by providing sensitivity and response analyses for nuclear energies and, for the first time, quadrupole moments, presented here for low-lying states of <sup>6</sup>Li and <sup>12</sup>C. Our results are made possible with the methodology of global sensitivity analysis (GSA) [23, 24], which is often prohibitively expensive since the number of model evaluations required for convergence grows rapidly with the number of model parameters. Fortunately, the symmetry-adapted no-core shell model (SA-NCSM) [25– 27] alleviates the cost of each evaluation by utilizing a fraction of ultra-large no-core shell model spaces without compromising the accuracy of the results. The SA-NCSM is an ab initio approach that has provided successful descriptions of electric quadrupole moments [25] and transition strengths without utilizing effective charges [14, 15, 28], energy spectra [29, 30], clustering features [29, 31, 32], and even reaction dynamics [25, 33–35], up through the calcium region. It produces the same results as the traditional no-core shell model [36, 37] for a given inter-nucleon interaction, characterized by the number of harmonic oscillator (HO) shells accessible to the nucleons, and the HO inter-shell energy  $\hbar\Omega$ .

Within this framework, we probe the response of collective features to short-distance NN coupling strengths, given by eleven LECs in chiral two-body potentials that are associated with the contact interactions of two nucleons for a given partial wave  $^{2S+1}\ell_J$ . These LECs are hence denoted as  $C_{^{2S+1}\ell_J}$ . Our new insights into the particular details of the nuclear force inform deformation and collectivity, and are therefore critical in advancing the frontier of high-precision nuclear simulations and uncertainty quantification that stem from the parametrizations of chiral potentials (see, e.g., [38–40]).

Resilience of nuclear shapes. - To study the responses of collective features to variations in the short-range coupling strengths, we start with the LEC parametrization of the NNLO<sub>opt</sub> chiral NN potential [41]. This potential is used without three-nucleon forces, which have been shown to contribute minimally to three- and four-nucleon binding energies [41], and is parametrized by 14 LECs from Feynman diagrams included up to next-to-next-toleading order (NNLO) in the chiral expansion. Furthermore, NNLO<sub>opt</sub> has been found to reproduce various observables and yield results equivalent to those obtained from chiral potentials that require three-nucleon forces, including, e.g., the <sup>4</sup>He electric dipole polarizability [42] and A = 8 energy spectra and quadrupole moments [29] (cf. Ref. [43] for A = 7.8 with the N<sup>3</sup>LO-EM chiral potential [17] with a corresponding, comparatively significant, three-nucleon force that decreases  $Q_2$  by up to

An NNLO chiral NN potential includes the following LECs: 11 contact couplings,  $C_{^{1}S_{0}(pp,np,nn),^{3}S_{1}}^{(LO)}$  at leading

order (LO),  $C_{^{1}S_{0},^{3}S_{1}}^{(\text{NLO})}$  and  $C_{^{3}S_{1}-^{3}D_{1},^{3}P_{0,1,2},^{1}P_{1}}$  at next-to-leading order (NLO), along with  $c_{1,3,4}$  at NNLO which parametrize parts of the two-pion exchange interaction (Fig. 2, inset). We note that NNLO<sub>opt</sub> does not include pure D-wave contact interactions as they emerge at the next chiral order (N3LO), and further note that by using NNLO<sub>opt</sub> this study adopts its regulator function and cutoff, variations of which are beyond the present scope. We vary these LECs, uniformly sampled using a Latin hypercube design [44], with each LEC bounded within  $\pm 10\%$  of its NNLO<sub>opt</sub> value.

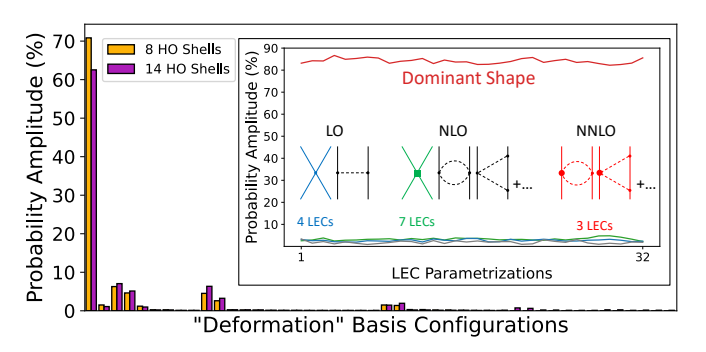


FIG. 2: Probability amplitudes of the "deformation" basis configurations of the  $^6\mathrm{Li}~1^+_\mathrm{g.s.}$  ground state calculated with NNLO\_{opt} in complete model spaces of 8 (yellow) and 14 (purple) HO shells (shown are contributions with probability amplitude  $\geq 0.1\%$ ). Inset: The four nuclear shapes with the largest probability amplitudes in the 8-shell  $^6\mathrm{Li}~1^+_\mathrm{g.s.}$  state across 32 NN parametrizations uniformly sampled within  $\pm 10\%$  around the NNLO\_opt LECs (see text for details). While not shown, the inset results remain practically unchanged for 1%-50% LEC variations [40, 45]. Also shown are the Feynman diagrams for chiral NN forces up to NNLO with the total number of LECs per order.

First, using NNLO<sub>opt</sub>, we perform SA-NCSM calculations –with no a priori approximations or assumptions– in the so-called "deformation" basis, known as the SU(3)adapted basis [26, 46], for complete model spaces, that is, with all possible basis states given the number of accessible HO shells. Clearly, as shown in Fig. 2 for the 1<sup>+</sup><sub>g.s.</sub> ground state of <sup>6</sup>Li, the probability amplitudes calculated in a model space of 8 HO shells vary only slightly compared to those calculated in the drastically larger model space spanned by 14 HO shells. Similar outcomes are observed for the energy  $E_{\rm X}$  of the first excited  $3_1^+$  state of <sup>6</sup>Li, as well as the quadrupole moments  $Q_2$  of the  $1_{\rm g.s.}^+$ and  $3_1^+$  (see Fig. 9 in the supplemental material). These results indicate that the 8-shell model spaces are sufficient for our GSA that requires hundreds of thousands of large-scale computations, especially since the focus here is on responses to variations in the LECs and the physics that tracks with such changes. In addition, without loss of generality, our calculations use a single  $\hbar\Omega = 15$  MeV, for which the rms radii converge comparatively faster [1].

A very interesting result emerges when we further

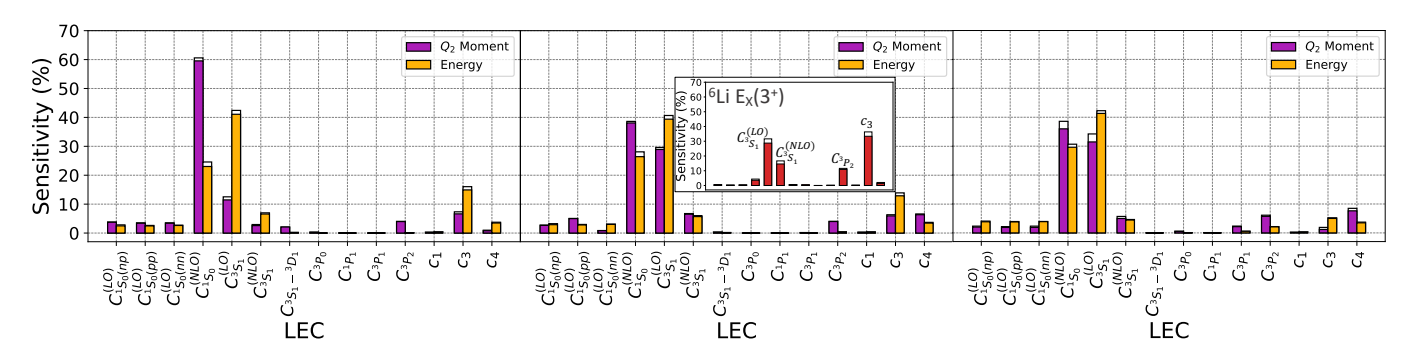


FIG. 3: First-order (colored) and total-order (white) sensitivity indices of the quadrupole moments (purple) and energies (yellow) of (a) the  $^6$ Li  $^+_{g.s.}$ , (b)  $^6$ Li  $^+_3$ , and (c)  $^{12}$ C  $^+_1$  states. Calculations use SA model spaces comprised of fourteen shapes spanning 8 HO shells. Inset: Sensitivity indices for the  $^6$ Li  $^+_3$  excitation energy,  $E_X(^3+)$ .

project these states onto the so-called "shape" basis, known as the Sp(3,  $\mathbb{R}$ )-adapted basis [1, 25–27]. Sp(3,  $\mathbb{R}$ )preserving subspaces represent nuclear shapes [3, 47, 48], each of which includes a static deformation and its dvnamical surface oscillations [multiples of  $2\hbar\Omega$  1-particle-1-hole (1p-1h) excitations, as illustrated in Fig. 1. Remarkably, as shown in the inset of Fig. 2, the shapes, and above all the dominant shape contributing 82.2-86.6% to the  $1_{g,s}^+$  state, are left practically untouched across the 10% LEC variations (see Fig. 6 of the supplemental material for all the states under consideration). We note that for the NNLO<sub>opt</sub> parametrization, the most dominant shape comprises about 86% of the <sup>6</sup>Li wave functions, whereas fourteen shapes recover about 97% of the total probabilities. In a simple picture of rigid shapes that rotate (as is assumed in Ref. [49]), the quadrupole moment will only vary as these probabilities vary [30, 48]. Given the resilience of the nuclear shapes to LEC variations, should one then expect merely marginal effects on quadrupole moments?

To answer this question, we first perform a global sensitivity analysis to probe whether  $Q_2$  is sensitive to changes in the LECs individually, or if the induced variance depends strongly on correlations between the LECs. If the correlations are small, we can then search for the underlying mechanism through the responses of  $Q_2$  to each LEC independently.

Sensitivity of collective observables.— We generate 300,000 samples in the LEC parameter space using Saltelli's procedure, implemented by the python library SALib [50, 51]. With the aid of high-performance computing, these parametrizations are used for the state-of-the-art evaluation of 300,000 nuclear simulations — only possible in the Sp(3,  $\mathbb{R}$ ) shape basis — of the energy and  $Q_2$  moment of the  $1^+_{g.s.}$  and  $3^+_1$  states of <sup>6</sup>Li, and the  $2^+_1$  state of <sup>12</sup>C. We find a pronounced sensitivity of  $Q_2$  to two singlet (spin-zero) and triplet (spin-one) S-wave contacts, namely,  $C^{(LO)}_{3S_1}$  and  $C^{(NLO)}_{1S_0}$  (Fig. 3). This is indicated by the first-order sensitivity indices  $S_i$ , quantifying the fractional variances in the samples due to the  $i^{th}$  LEC alone. In contrast to the excitation energies, this

is the same physics to which their binding energies are most sensitive, as earlier recognized in  $^{16}{\rm O}$  [52], suggesting that both the binding energy and quadrupole moment may simultaneously inform the LEC fitting.

To enable this huge number of calculations, required for convergence of the GSA results, we utilize symmetryadapted (SA) model spaces selected from fourteen shapes spanning 8 HO shells. We find that the resulting sensitivity patterns are practically unchanged across various model space selections and sizes, and show this for <sup>6</sup>Li in model spaces comprised of 1 shape, 14 shapes, and all possible shapes (corresponding to the complete model space), and in larger model spaces comprised of 10 and 12 HO shells in Figs. 7 and 8 of the supplemental material, respectively. Based on this validation and using the same shape-selection prescription, the sensitivity analysis becomes feasible for the  $^{12}{\rm C}$   $2_1^+$  state in SA model spaces consisting of fourteen shapes that account for about 80% of the state. In this way, one can utilize Hamiltonian matrices in the selected shape basis of highly reduced dimensions (e.g., four orders of magnitude reduction for the  $2_1^+$  state) that can serve as emulators, similarly to, e.g., Refs. [53–58]. Indeed, we find that the sensitivity patterns for <sup>12</sup>C [Fig. 3(c)] closely resemble those for

Importantly, the total-order sensitivity indices, which additionally include correlations with all remaining LECs, practically coincide with the first-order indices  $S_i$  (Fig. 3). This suggests that the main effect of each LEC on  $Q_2$  is largely decoupled from those of the remaining parameters, and can be explored separately. This is especially useful since the sensitivity indices are normalized to the total variance of the  $Q_2$  distributions sampled, and thus provide a relative contribution only. The degree to which each contact coupling affects  $Q_2$  can hence be understood by studying the responses of the LECs individually, as discussed next.

Short-range footprints on long-range physics.—We discover that nonnegligible nuclear quadrupole moments of collective states, such as the  $^6\mathrm{Li}~3_1^+$  and  $^{12}\mathrm{C}~2_1^+$  states, can be enhanced by nearly 50% through two competing S-wave contact interactions, which do so via an unex-

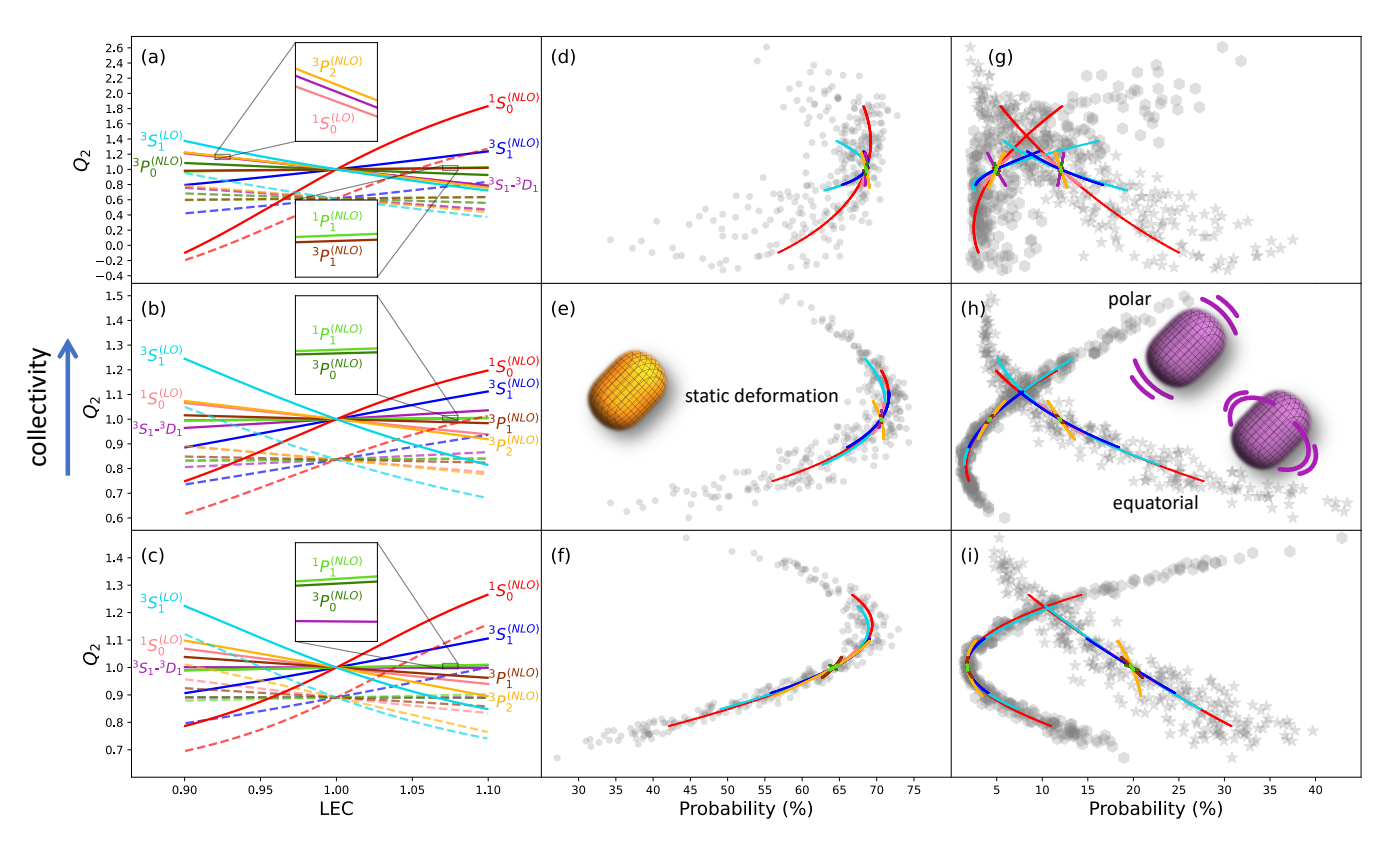


FIG. 4:  $Q_2$  quadrupole moment (solid), relative to their NNLO<sub>opt</sub> values, of (a) the <sup>6</sup>Li  $1_{g.s.}^+$ , (b) <sup>6</sup>Li  $3_1^+$ , and (c) <sup>12</sup>C  $2_1^+$  states vs. each LEC varied  $\pm 10\%$  around its NNLO<sub>opt</sub> value. Also shown is the  $Q_2$  contribution of the dominant shape (dashed). The corresponding probability amplitudes of the dominant shape are shown for (d)-(f) the static (0p-0h) deformation, together with (g)-(i) the surface oscillations along the symmetry axis (labeled "polar") and perpendicular to it (labeled "equatorial").  $Q_2$  moments obtained from 300 simultaneously varied LEC samples are shown in gray for the static (circles), polar (hexagons), and equatorial deformation (stars).

pected mechanism (Fig. 4). To show this, we first fix all LECs but one to their NNLO<sub>opt</sub> values, and draw 300 samples for each individual LEC, following a Latin hypercube design (Fig. 4, where for visual clarity we exclude the LO proton-proton and neutron-neutron  $^1S_0$  contacts, and since we focus on the contact physics, similarly exclude  $c_1$ ,  $c_3$ , and  $c_4$ ; for completeness, we provide all these in the supplemental material).

Corroborating the GSA results of Fig. 3, Fig. 4 unveils additionally interesting features, namely that  $Q_2$  depends practically linearly on the LECs, and that the S-wave contacts act in opposition: increasing the LO S-wave couplings (especially the triplet  $^3S_1$ ) of the attractive delta contact interaction decreases  $Q_2$ , while increasing the coupling strength of the repulsive NLO S-wave contact (dominated by the singlet  $^1S_0$ ) results in larger  $Q_2$  moments. We note that the stronger the LO  $^3S_1$  coupling, the more bound the deuteron system is, and that an attractive delta interaction has historically been used to describe pairing. Indeed, in phenomenological nuclear models, increasing the pairing strength leads to some decrease in  $Q_2$ , which actually results from a strong mixing of nuclear shapes [59]. Surprisingly, Fig. 4 shows such

a decrease in  $Q_2$ , but with practically no change in the mixing of the nuclear shapes, as illustrated in Fig. 2. This suggests that another mechanism might be responsible. Given the large probability amplitudes of the dominant nuclear shapes, we explore whether the observed variances are tied to changes within these dominant shapes. Importantly, since the total quadrupole moment is the sum of  $Q_2$  contributions from each nuclear shape (as  $Q_2$  does not couple different shapes), the component of  $Q_2$  attributed to the dominant shape not only yields most of the total  $Q_2$  value, but also exhibits nearly identical LEC dependence [Fig. 4, (a)–(c), dashed].

The physics of the dominant shape unveils, for the first time, the unexpected result that the S-wave contacts of the underlying chiral potential can significantly alter the magnitude of  $Q_2$  by impacting the shape's surface dynamics: the magnitude of  $Q_2$  increases for a stronger repulsive  $^1S_0$  contact interaction by favoring polar oscillations, that is, multiples of two HO quanta along the symmetry axis, and decreases as the equatorial modes (having HO quanta in the plane perpendicular to the symmetry axis) become dominant with a more attractive  $^3S_1$  contact [Fig. 4(g)-(i)]. This can be understood as fol-

lows: the  $^1S_0$  contact, by spreading nucleons to higher HO shells, reduces Pauli principle constraints and makes prolate (football-like) configurations accessible, and these are known to have low kinetic energy [60, 61] (Fig. 5). In contrast to this, as the LO  $^3S_1$  coupling of the delta contact increases, excitations in the equatorial planes become favorable, leading to a further decrease of the negative potential energy (Fig. 5); and while this results in larger binding energy, it comes at the expense of reduced collectivity.

These two contacts together can impact  $Q_2$  by up to  $\sim 50\%$  for the <sup>6</sup>Li  $3_1^+$  and <sup>12</sup>C  $2_1^+$  collective states (see Fig. 5 for the  $3_1^+$  state), compared to, e.g., 2-15% manybody model uncertainties in the present GSA calculations (cf. Refs. [62, 63] for the infinite-space estimates using NNLO<sub>opt</sub> for <sup>6</sup>Li and <sup>12</sup>C; in addition, Ref. [63] reports 13% many-body model uncertainties in the ab initio estimate for  $Q_2$ ). Furthermore, the importance of the polar modes cannot be understated: whether the equilibrium deformation is prolate as in <sup>6</sup>Li, or oblate as in <sup>12</sup>C, only polar oscillations will enhance collectivity. In short, we link the impact of the short-distance contact physics on nuclear collectivity to the surface dynamics that can increase (decrease)  $Q_2$  predominantly through a stronger repulsive NLO (attractive LO) S-wave contact that favors polar (equatorial) oscillations, which lower the kinetic (potential) energy. This impact is not merely marginal, which in turn makes quadrupole moments important observables to constrain realistic nuclear forces.

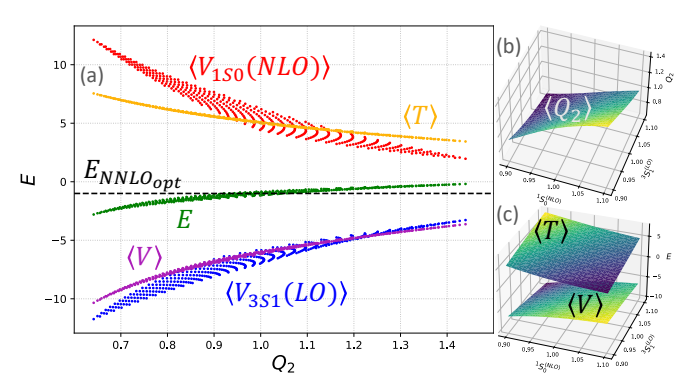


FIG. 5: (a) The energy E of the  $^6\mathrm{Li}\ 3_1^+$  state (green), the expectation value of the total potential energy  $\langle V \rangle$  (purple) and total kinetic energy  $\langle T \rangle$  (yellow), as well as of the LO  $^3S_1$  and NLO  $^1S_0$  potentials (blue and red, respectively), as functions of the electric quadrupole moment  $Q_2$ . The quadrupole moments are normalized to their NNLO<sub>opt</sub> values, while the expectation values are all normalized to the NNLO<sub>opt</sub> energy of the  $3_1^+$  state,  $E_{\mathrm{NNLO}_{\mathrm{opt}}}$ . (b) The quadrupole moment and (c)  $\langle T \rangle$  and  $\langle V \rangle$  vs. the LO  $^3S_1$  and NLO  $^1S_0$  contact couplings.

To summarize, we find that electric quadrupole moments of light deformed nuclei, which provide a measure of their collectivity, are sensitive to short-range chiral contact NN interactions, namely, two opposing attractive triplet and repulsive singlet S-wave contacts. While historically larger  $Q_2$  moments have been associated with reduced mixing between nuclear shapes or shapes of larger deformation, here, for the first time, we show that contact interactions can significantly increase the magnitude of  $Q_2$  by subtly altering the surface dynamics of (typically) one dominant nuclear shape. We show that quadrupole collectivity is maximized by enhancing the polar surface oscillations at the expense of the remaining excitations, and this is most readily accomplished by increasing the magnitude of the  ${}^{1}S_{0}$  coupling or decreasing that of the  ${}^{3}S_{1}$  contact. We have thus found a direct link between an ab initio description of nuclear collectivity and the short-range part of the underlying strong forces between nucleons which are rooted in QCD. This, in turn, paves the way for the construction of chiral potentials that can predict collective properties of atomic nuclei, while at the same time shedding new light on the emergent collectivity that dominates nuclear dynamics.

### ACKNOWLEDGMENTS

This work was supported by the U.S. Department of Energy (DE-SC0023532), the European Research Council (ERC) under the European Union's Horizon 2020 research and innovation program (Grant Agreement No. 758027), the Swedish Research Council (Grant Agreement No. 2020-05127), and the Czech Science Foundation (22-14497S). This material is based upon work supported by the U.S. Department of Energy, Office of Science, Office of Nuclear Physics, under the FRIB Theory Alliance award DE-SC0013617. This work benefited from high performance computational resources provided by LSU (www.hpc.lsu.edu), the National Energy Research Scientific Computing Center (NERSC), a U.S. Department of Energy Office of Science User Facility at Lawrence Berkeley National Laboratory operated under Contract No. DE-AC02-05CH11231, as well as the Frontera computing project at the Texas Advanced Computing Center, made possible by National Science Foundation award OAC-1818253.

T. Dytrych, K. D. Launey, J. P. Draayer, D. J. Rowe, J. L. Wood, G. Rosensteel, C. Bahri, D. Langr, and R. B.

- [2] A. Bohr and B. R. Mottelson, Nuclear Structure, Vol. 1 (Benjamin, New York, 1969).
- [3] D. J. Rowe, The emergence and use of symmetry in the many-nucleon model of atomic nuclei, in *Emergent phe*nomena in atomic nuclei from large-scale modeling: a symmetry-guided perspective (World Scientific Publishing Co., 2017) p. 65.
- [4] K. Heyde and J. L. Wood, Shape coexistence in atomic nuclei, Rev. Mod. Phys. 83, 1467 (2011).
- [5] P. E. Garrett, M. Zielińska, and E. Clément, An experimental view on shape coexistence in nuclei, Progress in Particle and Nuclear Physics 124, 103931 (2022).
- [6] T. Gray, J. Allmond, R. Janssens, W. Korten, A. Stuchbery, J. Wood, A. Ayangeakaa, S. Bottoni, B. Bucher, C. Campbell, M. Carpenter, H. Crawford, H. David, D. Doherty, P. Fallon, M. Febbraro, A. Galindo-Uribarri, C. Gross, M. Komorowska, F. Kondev, T. Lauritsen, A. Macchiavelli, P. Napiorkowsi, E. Padilla-Rodal, S. Pain, W. Reviol, D. Sarantites, G. Savard, D. Seweryniak, C. Wu, C.-H. Yu, and S. Zhu, E2 rotational invariants of 0<sup>+</sup><sub>1</sub> and 2<sup>+</sup><sub>1</sub> states for 106cd: The emergence of collective rotation, Physics Letters B 834, 137446 (2022).
- [7] D. Ivanova, S. Lalkovski, L. Atanasova, S. Kisyov, I. Vasilev, C. Mihai, A. Turturica, A. Blazhev, R. Borcea, M. Boromiza, S. Calinescu, C. C. Stan, C. Costache, A. Gandhi, D. Grigorova, R. Lica, N. Marginean, R. Marginean, C. Müller-Gatermann, A. Olacel, N. L. Petrov, L. Stan, E. A. Stefanova, I. Stiru, G. Stoev, S. Toma, G. Turturica, S. Ujeniuc, and O. Yordanov, Core-excited states in 105cd, Physica Scripta 99, 075316 (2024).
- [8] A. Spătaru, G. Kripko-Koncz, D. Amanbayev, S. A. S. Andrés, D. L. Balabanski, S. Beck, J. Bergmann, P. Constantin, T. Dickel, H. Geissel, C. Hornung, N. Kalantar-Nayestanaki, I. Mardor, N. Minkov, A. Mollaebrahimi, W. R. Plaß, C. Scheidenberger, M. Wasserheß, and J. Zhao, Studying shape phase transition in even-proton nuclei via mass measurements, Physica Scripta 99, 075305 (2024).
- [9] G. Riczu, J. Darai, and J. Cseh, Superdeformation and dynamical symmetry, Physica Scripta 99, 045306 (2024).
- [10] R. Benjedi, R. Budaca, P. Buganu, Y. E. Bassem, A. Lahbas, and M. Oulne, Shapes and structure for the lowest states of the 42,44ca isotopes, Physica Scripta 99, 055307 (2024).
- [11] K. A. Gladnishki, L. Atanasova, A. Blazhev, M. Djongolov, G. Georgiev, N. Ivanov, D. Kalaydjieva, D. Kocheva, R. Lozeva, G. Rainovski, M. Stoyanova, and K. Stoychev, Electromagnetic transition rates in the nucleus 13658ce, Physica Scripta 99, 065305 (2024).
- [12] D. Kocheva, G. Rainovski, J. Jolie, M. Beckers, A. Blazhev, A. Esmaylzadeh, C. Fransen, K. A. Gladnishki, N. Pietralla, M. Scheck, F. Spee, M. Stoyanova, V. Werner, G. D. Gregorio, A. Gargano, and B. A. Brown, Study the structure of the low-lying states of 206po, Physica Scripta 99, 065307 (2024).
- [13] A. V. Afanasjev, S. Teeti, and A. Taninah, Fast rotation of nuclei with extreme isospin in the vicinity of neutron and proton drip lines, Physica Scripta 99, 065313 (2024).
- [14] J. Henderson et al., Testing microscopically derived descriptions of nuclear collectivity: Coulomb excitation of <sup>22</sup>Mg, Phys. Lett. B782, 468 (2018), arXiv:1709.03948 [nucl-ex].
- [15] P. Ruotsalainen, J. Henderson, G. Hackman, G. H.

- Sargsyan, K. D. Launey, A. Saxena, P. C. Srivastava, S. R. Stroberg, T. Grahn, J. Pakarinen, G. C. Ball, R. Julin, P. T. Greenlees, J. Smallcombe, C. Andreoiu, N. Bernier, M. Bowry, M. Buckner, R. Caballero-Folch, A. Chester, S. Cruz, L. J. Evitts, R. Frederick, A. B. Garnsworthy, M. Holl, A. Kurkjian, D. Kisliuk, K. G. Leach, E. McGee, J. Measures, D. Mücher, J. Park, F. Sarazin, J. K. Smith, D. Southall, K. Starosta, C. E. Svensson, K. Whitmore, M. Williams, and C. Y. Wu, Isospin symmetry in b(e2) values: Coulomb excitation study of <sup>21</sup>Mg, Phys. Rev. C **99**, 051301 (2019).
- [16] P. F. Bedaque and U. van Kolck, Effective field theory for few-nucleon systems, Annu. Rev. Nucl. Part. Sci. 52, 339 (2002).
- [17] D. R. Entem and R. Machleidt, Phys. Rev. C 68, 041001 (2003).
- [18] E. Epelbaum, H. Krebs, and U. G. Meißner, Precision nucleon-nucleon potential at fifth order in the chiral expansion, Phys. Rev. Lett. 115, 122301 (2015), arXiv:1412.4623 [nucl-th].
- [19] H.-W. Hammer, S. König, and U. van Kolck, Nuclear effective field theory: Status and perspectives, Rev. Mod. Phys. 92, 025004 (2020).
- [20] C. McIlroy, C. Barbieri, T. Inoue, T. Doi, and T. Hatsuda, Doubly magic nuclei from lattice qcd forces at  $M_{\rm ps} = 469\,{\rm MeV}/c^2$ , Phys. Rev. C **97**, 021303 (2018).
- [21] I. Tews, Z. Davoudi, A. Ekström, J. D. Holt, and J. E. Lynn, New ideas in constraining nuclear forces, Journal of Physics G: Nuclear and Particle Physics 47, 103001 (2020).
- [22] R. A. Briceño, Z. Davoudi, T. C. Luu, and M. J. Savage, Two-nucleon systems in a finite volume. ii.  ${}^3s_1 {}^3d_1$  coupled channels and the deuteron, Phys. Rev. D **88**, 114507 (2013).
- [23] I. Sobol', Global sensitivity indices for nonlinear mathematical models and their monte carlo estimates, Mathematics and Computers in Simulation 55, 271 (2001), the Second IMACS Seminar on Monte Carlo Methods.
- [24] A. Saltelli, P. Annoni, I. Azzini, F. Campolongo, M. Ratto, and S. Tarantola, Variance based sensitivity analysis of model output. design and estimator for the total sensitivity index, Computer Physics Communications 181, 259 (2010).
- [25] K. D. Launey, A. Mercenne, and T. Dytrych, Nuclear dynamics and reactions in the ab initio symmetry-adapted framework, Annu. Rev. Nucl. Part. Sci. 71, 253 (2021).
- [26] K. D. Launey, T. Dytrych, and J. P. Draayer, Symmetry-guided large-scale shell-model theory, Prog. Part. Nucl. Phys. 89, 101 (review) (2016).
- [27] T. Dytrych, K. D. Sviratcheva, C. Bahri, J. P. Draayer, and J. P. Vary, Evidence for Symplectic Symmetry in ab initio No-core-shell-model Results for Light Nuclei, Phys. Rev. Lett. 98, 162503 (2007).
- [28] J. Williams, G. C. Ball, A. Chester, T. Domingo, A. B. Garnsworthy, G. Hackman, J. Henderson, R. Henderson, R. Krücken, A. Kumar, K. D. Launey, J. Measures, O. Paetkau, J. Park, G. H. Sargsyan, J. Smallcombe, P. C. Srivastava, K. Starosta, C. E. Svensson, K. Whitmore, and M. Williams, Structure of <sup>28</sup>Mg and influence of the neutron pf shell, Phys. Rev. C 100, 014322 (2019).
- [29] G. H. Sargsyan, K. D. Launey, M. T. Burkey, A. T. Gallant, N. D. Scielzo, G. Savard, A. Mercenne, T. Dytrych, D. Langr, L. Varriano, B. Longfellow, T. Y. Hirsh, and J. P. Draayer, Impact of clustering on the <sup>8</sup>Li β decay and

- recoil form factors, Phys. Rev. Lett. 128, 202503 (2022).
- [30] N. D. Heller, G. H. Sargsyan, K. D. Launey, C. W. Johnson, T. Dytrych, and J. P. Draayer, New insights into backbending in the symmetry-adapted shell-model framework, Phys. Rev. C 108, 024304 (2023).
- [31] A. C. Dreyfuss, K. D. Launey, J. E. Escher, G. H. Sargsyan, R. B. Baker, T. Dytrych, and J. P. Draayer, Clustering and  $\alpha$ -capture reaction rate from ab initio symmetry-adapted descriptions of  $^{20}$ Ne, Phys. Rev. C **102**, 044608 (2020).
- [32] A. C. Dreyfuss, K. D. Launey, T. Dytrych, J. P. Draayer, R. B. Baker, C. M. Deibel, and C. Bahri, Understanding emergent collectivity and clustering in nuclei from a symmetry-based no-core shell-model perspective, Phys. Rev. C 95, 044312 (2017).
- [33] A. Mercenne, K. D. Launey, J. E. Escher, T. Dytrych, and J. P. Draayer, New Ab Initio Approach to Nuclear Reactions Based on the Symmetry-Adapted No-Core Shell Model, in *Recent Progress in Few-Body Physics*, Vol. 238, edited by N. Orr, M. Ploszajczak, F. Marques, and J. Carbonell (Springer Proc. Phys., 2020) p. 253.
- [34] A. Mercenne, K. Launey, T. Dytrych, J. Escher, S. Quaglioni, G. Sargsyan, D. Langr, and J. Draayer, Efficacy of the symmetry-adapted basis for ab initio nucleonnucleus interactions for light- and intermediate-mass nuclei, Computer Physics Communications 280, 108476 (2022).
- [35] M. Burrows, R. B. Baker, S. Bacca, K. D. Launey, T. Dytrych, and D. Langr, Response functions and giant monopole resonances for light to medium-mass nuclei from the *ab initio* symmetry-adapted no-core shell model (2023), arXiv:2312.09782.
- [36] P. Navrátil, J. P. Vary, and B. R. Barrett, Properties of <sup>12</sup>C in the *Ab Initio* Nuclear Shell Model, Phys. Rev. Lett. 84, 5728 (2000).
- [37] B. Barrett, P. Navrátil, and J. Vary, Prog. Part. Nucl. Phys. 69, 131 (2013).
- [38] B. D. Carlsson, A. Ekström, C. Forssén, D. F. Strömberg, G. R. Jansen, O. Lilja, M. Lindby, B. A. Mattsson, and K. A. Wendt, Uncertainty analysis and order-by-order optimization of chiral nuclear interactions, Phys. Rev. X 6, 011019 (2016).
- [39] I. Svensson, A. Ekström, and C. Forssén, Bayesian estimation of the low-energy constants up to fourth order in the nucleon-nucleon sector of chiral effective field theory, Phys. Rev. C 107, 014001 (2023).
- [40] K. S. Becker, K. D. Launey, A. Ekström, T. Dytrych, D. Langr, G. H. Sargsyan, and J. P. Draayer, Uncertainty quantification of collective nuclear observables from the chiral potential parametrization (2024), arXiv:2404.00063.
- [41] A. Ekström, G. Baardsen, C. Forssén, G. Hagen, M. Hjorth-Jensen, G. R. Jansen, R. Machleidt, W. Nazarewicz, et al., An optimized chiral nucleon-nucleon interaction at next-to-next-to-leading order, Phys. Rev. Lett. 110, 192502 (2013).
- [42] R. B. Baker, K. D. Launey, S. Bacca, N. N. Dinur, and T. Dytrych, Benchmark calculations of electromagnetic sum rules with a symmetry-adapted basis and hyperspherical harmonics, Phys. Rev. C 102, 014320 (2020).
- [43] P. Maris, J. P. Vary, and P. Navrátil, Phys. Rev. C 87, 014327 (2013).
- [44] M. D. Mckay, R. J. Beckman, and W. J. Conover, A comparison of three methods for selecting values of input

- variables in the analysis of output from a computer code, Technometrics **42**, 55 (2000).
- [45] K. S. Becker, K. D. Launey, A. Ekström, G. H. Sargsyan, D. C. Mumma, T. Dytrych, D. Langr, and J. P. Draayer, Understanding the effect of chiral nn parametrization on nuclear shapes from an ab initio perspective (2023), arXiv:2311.13020.
- [46] K. D. Launey, T. Dytrych, G. H. Sargsyan, R. B. Baker, and J. P. Draayer, Emergent symplectic symmetry in atomic nuclei: *Ab initio* symmetry-adapted no-core shell model, Eur. Phys. J. Spec. Top. 229, 2429 (2020).
- [47] G. Rosensteel and D. J. Rowe, Nuclear Sp(3,R) Model, Phys. Rev. Lett. 38, 10 (1977).
- [48] D. J. Rowe, Microscopic theory of the nuclear collective model, Reports on Progr. in Phys. 48, 1419 (1985).
- [49] Z. H. Sun, A. Ekström, C. Forssén, G. Hagen, G. R. Jansen, and T. Papenbrock, Multiscale physics of atomic nuclei from first principles (2024), arXiv:2404.00058 [nucl-th].
- [50] T. Iwanaga, W. Usher, and J. Herman, Toward SALib 2.0: Advancing the accessibility and interpretability of global sensitivity analyses, Socio-Environmental Systems Modelling 4, 18155 (2022).
- [51] J. Herman and W. Usher, SALib: An open-source python library for sensitivity analysis, The Journal of Open Source Software 2, 10.21105/joss.00097 (2017).
- [52] A. Ekström and G. Hagen, Global sensitivity analysis of bulk properties of an atomic nucleus, Phys. Rev. Lett. 123, 252501 (2019), arXiv:1910.02922.
- [53] D. Odell, P. Giuliani, K. Beyer, M. Catacora-Rios, M. Y. H. Chan, E. Bonilla, R. J. Furnstahl, K. Godbey, and F. M. Nunes, Rose: A reduced-order scattering emulator for optical models (2023), arXiv:2312.12426 [physics.comp-ph].
- [54] T. Djärv, A. Ekström, C. Forssé n, and H. T. Johansson, Bayesian predictions for a = 6 nuclei using eigenvector continuation emulators, Phys. Rev. C 105, 10.1103/physrevc.105.014005 (2022), arXiv:2108.13313.
- [55] K. S. Becker, K. D. Launey, A. Ekstrom, and T. Dytrych, Ab initio symmetry-adapted emulator for studying emergent collectivity and clustering in nuclei, Front. Phys. 11, 1064601 (2023).
- [56] S. König, A. Ekström, K. Hebeler, D. Lee, and A. Schwenk, Eigenvector continuation as an efficient and accurate emulator for uncertainty quantification, Physics Letters B 810, 135814 (2020), arXiv:1909.08446.
- [57] D. Frame, R. He, I. Ipsen, D. Lee, D. Lee, and E. Rrapaj, Eigenvector continuation with subspace learning, Phys. Rev. Lett. 121, 032501 (2018), arXiv:1711.07090.
- [58] T. Duguet, A. Ekström, R. J. Furnstahl, S. König, and D. Lee, Colloquium: Eigenvector continuation and projection-based emulators, Rev. Mod. Phys. 96, 031002 (2024).
- [59] J. Escher, C. Bahri, D. Troltenier, and J. Draayer, Pairing-plus-quadrupole model and nuclear deformation: A look at the spin-orbit interaction, Nuclear Physics A 633, 662 (1998).
- [60] B. Castel, D. Rowe, and L. Zamick, Why are deformed nuclei prolate?, Physics Letters B 236, 121 (1990).
- [61] D. Rowe, How do deformed nuclei rotate?, Nuclear Physics A 152, 273 (1970).
- [62] I. J. Shin, Y. Kim, P. Maris, J. P. Vary, C. Forssén, J. Rotureau, and N. Michel, Ab initio no-core solutions for <sup>6</sup>Li, J. Phys. G: Nucl. Part. Phys. 44, 075103 (2017).

- [63] G. H. Sargsyan, Electromagnetic Transitions and Beta Decays in Nuclei from the Ab initio Symmetry-adapted No-core Shell Model, Phd thesis, Louisiana State University, Example City, CA (2021), ISU Doctoral Dissertations, 5641, https://repository.lsu.edu/gradschool\_ dissertations/5641.
- [64] A. Saltelli, Making best use of model evaluations to compute sensitivity indices, Computer Physics Communications 145, 280 (2002).
- [65] T. Homma and A. Saltelli, Importance measures in global sensitivity analysis of nonlinear models, Reliability Engineering & System Safety 52, 1 (1996).
- [66] B. J. Verhaar, A Method for the Elimination of Spurious States in the Nuclear Harmonic Oscillator Shell Model, Nucl. Phys. 21, 508 (1960).
- [67] K. T. Hecht, Use of SU(3) in Elimination of Spurious Center of Mass States, Nucl. Phys. A 170, 34 (1971).
- [68] T. Dytrych, K. D. Launey, J. P. Draayer, P. Maris, J. P. Vary, E. Saule, U. Catalyurek, M. Sosonkina, D. Langr, and M. A. Caprio, Collective Modes in Light Nuclei from First Principles, Phys. Rev. Lett. 111, 252501 (2013).

### I. SUPPLEMENTAL MATERIALS

#### A. Sobol' global sensitivity analysis (GSA)

For completeness, we provide a brief overview of Sobol' sensitivity analysis (for further details, we refer the reader to the works of Sobol' and Saltelli, e.g., [23, 24, 64]). The basic premise is to determine how uncertainty in the inputs of a given model induce uncertainties in its output, at various orders of correlation. In order to fully explore these high-dimensional correlations, we employ a quasi-random sampling technique based on Sobol' sequences developed by A. Saltelli. This method generates a set of inputs that efficiently fills the entire hypervolume of the parameter space and each lower-dimensional surface, according to the desired sample size (300,000 in our study) and the allowed ranges of each parameter. This allows for a comparatively fast calculation of the Sobol' sensitivity indices, which become increasingly more difficult to compute at higher orders. via Monte Carlo integration. This is especially useful for the so-called total-order effects or indices, which can be well approximated with a single integral rather than through explicit summation of all lower-order terms [65].

The Sobol' indices themselves are defined as the fractional variances of the sampled model outputs when considering variations on a subset of its inputs, achieved by decomposing the total sample variance  $\mathcal{V}$  in the following way:

$$\mathcal{V} = \sum_{i} \mathcal{V}_i + \sum_{i,j} \mathcal{V}_{ij} + \dots + \mathcal{V}_{ij\dots d},\tag{1}$$

where d=14 is the dimension of the parameter space,  $\mathcal{V}_i$  corresponds to the partial variance due to only the  $i^{\rm th}$  LEC,  $\mathcal{V}_{ij}$  arises through simultaneous variations of the  $i^{\rm th}$  and  $j^{\rm th}$  LECs, etc. The Sobol' indices are computed

by dividing these partial variances by the total variance  $\mathcal{V}$ , thus the first-order indices  $S_i$  are given by  $\mathcal{V}_i/\mathcal{V}$ , the second-order indices by  $\mathcal{V}_{ij}/\mathcal{V}$ , and so on. The total-order effect for parameter i is hence obtained by summing all fractional variances indexed by i, i.e.,

$$S_{Ti} = S_i + \sum_j S_{ij} + \sum_{j,k} S_{ijk} + \dots + S_{ij\dots d},$$
 (2)

though as mentioned this demanding sum is approximated with a single Monte Carlo integration (for further technical details, we refer to [64, 65]). Sobol' analysis is nonetheless extremely computationally intensive for large parameter spaces, as is the case in this work, and the need to lower the cost of individual model evaluations without sacrificing accuracy quickly becomes evident.

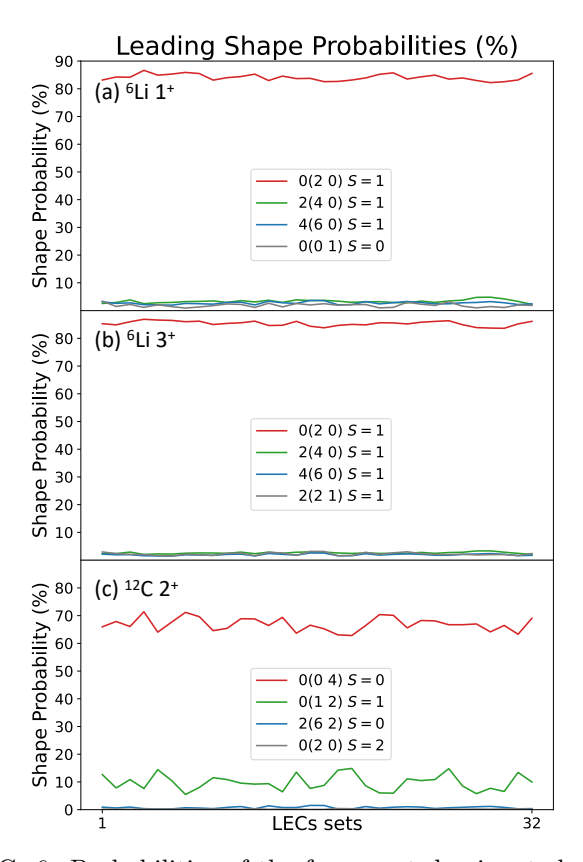


FIG. 6: Probabilities of the four most dominant shapes in (a) the <sup>6</sup>Li 1<sup>+</sup><sub>g.s.</sub> ground state, (b) its first excited 3<sup>+</sup><sub>1</sub> state, and (c) the first excited 2<sup>+</sup><sub>1</sub> state of <sup>12</sup>C, across the same 32 parametrizations shown in the inset of Fig. 2. The wavefunctions for all three states are calculated with  $\hbar\Omega = 15$  MeV and complete 8-shell HO model spaces. Each shape is labeled by the quantum numbers of its Sp(3,  $\mathbb{R}$ ) irreducible representation:  $N_{\sigma}(\lambda \mu)_{\sigma} S$ , where  $N_{\sigma}$  is the total number of HO quanta for the static deformation (with  $N_{\sigma} = 0$  denoting the valence shell),  $(\lambda \mu)_{\sigma}$  indicates the SU(3) quantum numbers describing the static deformation, and S is the total intrinsic spin.

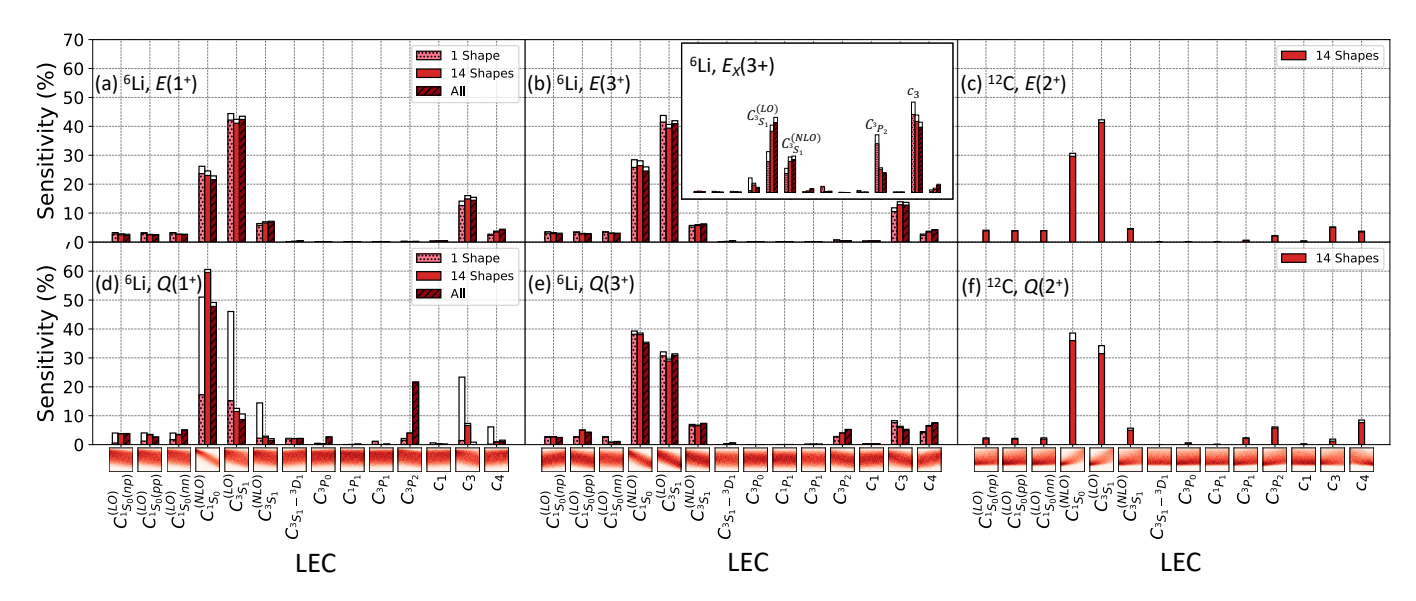


FIG. 7: First-order (colored) and total-order (white) sensitivity indices of the energies (top panels) and quadrupole moments (bottom panels) of the (a) & (d) <sup>6</sup>Li 1<sup>+</sup><sub>g.s.</sub>, (b) & (e) <sup>6</sup>Li 3<sup>+</sup><sub>1</sub>, and (c) & (f) <sup>12</sup>C 2<sup>+</sup><sub>1</sub> states. Calculations use SA model spaces comprised of 1 shape (light red, dotted; labeled as "1 Shape"), fourteen shapes (red, solid; "14 Shapes"), and all possible shapes (dark red, slashed; "All", which is the complete no-core shell-model space) spanning 8 HO shells. Histograms of the sampled LEC values and quadrupole moments divided into equally-spaced bins are shown at the bottom. Inset: Sensitivity indices for the <sup>6</sup>Li excitation energy,  $E_X$ , for the 3<sup>+</sup><sub>1</sub> state.

# B. Dominant shapes in chiral potential parametrizations

By organizing conventional no-core shell model spaces into symmetry-preserving subspaces of definite shape ("shape" basis configurations), the SA-NCSM reveals nature's striking preference for symmetry in light- and medium-mass nuclei [1, 25]. This enables accurate calculations of nuclear observables using mere fractions of ultra-large conventional model spaces through the procedure of shape selection. Furthermore, since the approach utilizes laboratory particle coordinates, the "shape" basis allows for an exact factorization of the center-of-mass motion, and states contaminated by spurious center-of-mass excitations are easily removed [66, 67].

For completeness, we demonstrate in Fig. 6 the resiliency of the most dominant nuclear shapes in the  $3_1^+$ and  $2_1^+$  states, and compare to the results shown for the  $1_{g.s.}^+$  in Fig. 2 in the main article. The same set of 32 uniformly-sampled LECs sets are used for each calculation. It is clear that symplectic symmetry is a very good symmetry in all three states, as it is always the same shape that dominates even if its probability fluctuates. The results for the  $3_1^+$  are extremely similar to those of the  $1_{\rm g.s.}^+$ , with a prolate shape contributing  $\geq 80\%$  for all LEC samples, and the next most-dominant shapes contribute < 10% each. In <sup>12</sup>C, it is an oblate shape that dominates at approximately a  $60\% \sim 70\%$  level, while the second most impactful shape is near-oblate and contributes between approximately  $5\% \sim 15\%$ . The remaining two shapes are barely visible, and their probabilities

fluctuate less appreciably than the first two.

# C. Convergence of sensitivity indices with shape selection

To determine the impact of shape selection on the sensitivity results, we perform the same analysis of the <sup>6</sup>Li states in two additional SA model spaces consisting of all possible shapes (i.e., the complete no-core shell model space) and the single most dominant shape alone (respectively labeled "All" and "1 shape" in Fig. 7), both expanded up to 8 HO shells. Clearly, Fig. 7 shows that the complete model spaces yield very similar sensitivity indices to those calculated with the fourteen shapes discussed in the text and reported in Fig. 3. In addition, in all cases of Fig. 7(a), (b), & (e), the sensitivity pattern remains the same even in the case of a single (dominant) shape. This is highly significant, strongly hinting that the observed variances are tied to changes in the deformed configurations belonging to that dominant shape, as demonstrated in Fig. 4.

We note that the  $Q_2(1_{\rm g.s.}^+)$  moment for  $^6{\rm Li}$  [Fig. 7(d)] exhibits some dependence on the model-space selection, e.g., the complete space yields different variances for  $C_{^3P_2}$  and  $c_3$ . Further, the large differences between the first-and total-order indices when considering only the dominant shape suggest correlations between the LECs, likely because of the limited number of available configurations. These differences may stem from the fact that the wave function is predominantly L=0 with small mixing from L=2 configurations ( $\sim 10\%$ ). Since the  $Q_2$  operator

cannot couple two states with L=0, its expectation value is close to zero and highly attuned to the extent and composition of the L=2 admixture [68], suggesting greater sensitivity to this mixing. This results in a  $Q_2(1_{\rm g.s.}^+)$  that is two orders of magnitude smaller compared to the  $^6{\rm Li}$   $3_1^+$  and  $^{12}{\rm C}$   $2_1^+$  collective states.

#### D. Convergence with model space size

To ensure that our results do not depend strongly on the number of included HO shells, we extend the 14-shape sensitivity analysis of the quadrupole moment for the  $^6\mathrm{Li}$   $3_1^+$  state to 10 shells, and the  $1_{\mathrm{g.s.}}^+$  state to 12 shells, that is, to larger model space sizes (Fig. 8). Clearly, the first-and total-order sensitivity indices for the quadrupole moments of both states are well converged.

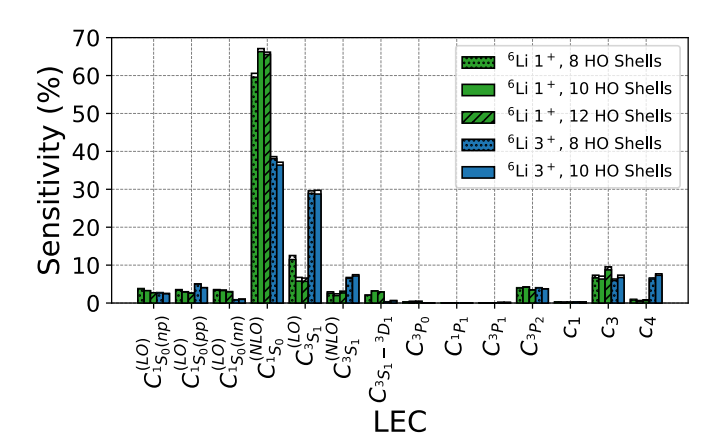


FIG. 8: First-order (colored) and total-order (white) sensitivity indices of the quadrupole moments sampled in the  $^6\mathrm{Li}\ 1_{\mathrm{g.s.}}^+$  (green) and first excited  $3_1^+$  states (blue). The shading patterns correspond to the 14-shape SA-model space expanded up to 8 (dotted), 10 (solid), and 12 (slashed) HO shells.

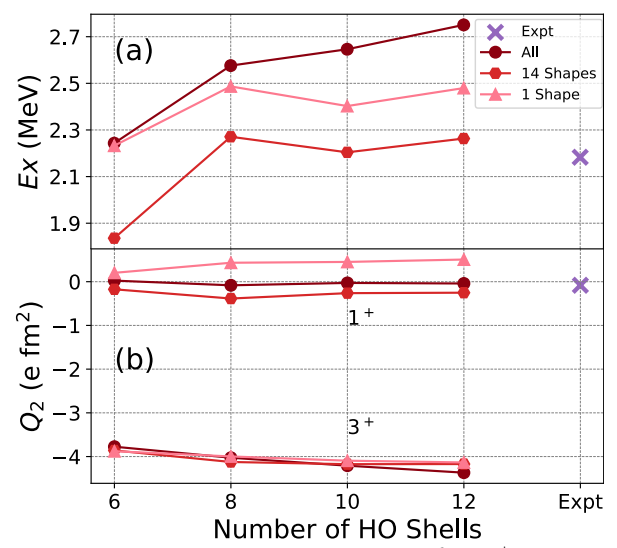


FIG. 9: (a) Excitation energy of the  $^6\mathrm{Li}\ 3_1^+$  state as a function of the number of included HO shells, in SA spaces spanned by the most dominant shape (pink triangles), fourteen shapes (red hexagons), and all shapes (crimson circles). (b) The quadrupole moment of the  $1_{\mathrm{g.s.}}^+$  (top) and  $3_1^+$  (bottom) states as a function of the number of included HO shells. All calculations use the NNLO<sub>opt</sub> LEC parametrization and  $\hbar\Omega=15$  MeV. Experimental data is shown with purple crosses where available.

In addition, we show that the  $^6\text{Li}\ 3_1^+$  excitation energy along with the quadrupole moment for the  $3_1^+$  and  $1_{\text{g.s.}}^+$  states, calculated using NNLO<sub>opt</sub>, exhibit converging trends with respect to the number of HO shells included, for all shape selections considered (Fig. 9).

For the sake of completeness, we additionally show in Fig. 10 how the total and single-shape  $Q_2$  moments of the  $^6\text{Li}\ 1^+_{\text{g.s.}}$  and  $^{12}\text{C}\ 2^+_1$  states depend on the LECs excluded from Fig. 4: the proton-proton and neutron-neutron components of  $C^{(LO)}_{^1S_0}$ , and the two-pion exchange LECs  $c_1, c_3$ , and  $c_4$  (while not shown, the outcome is similar for the  $3^+_1$  state of  $^6\text{Li}$ ). We also include the proton-neutron component of  $C^{(LO)}_{^1S_0}$  previously shown in Fig. 4, to illustrate the minimal effect of isospin-invariance breaking in the leading order  $^1S_0$  interaction. This set of LECs shown in Fig. 10 exerts only a marginal effect on both sets of quadrupole moments, especially compared to the dominant NLO  $^1S_0$  and LO  $^3S_1$  terms discussed in the main article (we note that the scale of the y-axis in Fig. 10 is smaller than the one in Fig. 4).

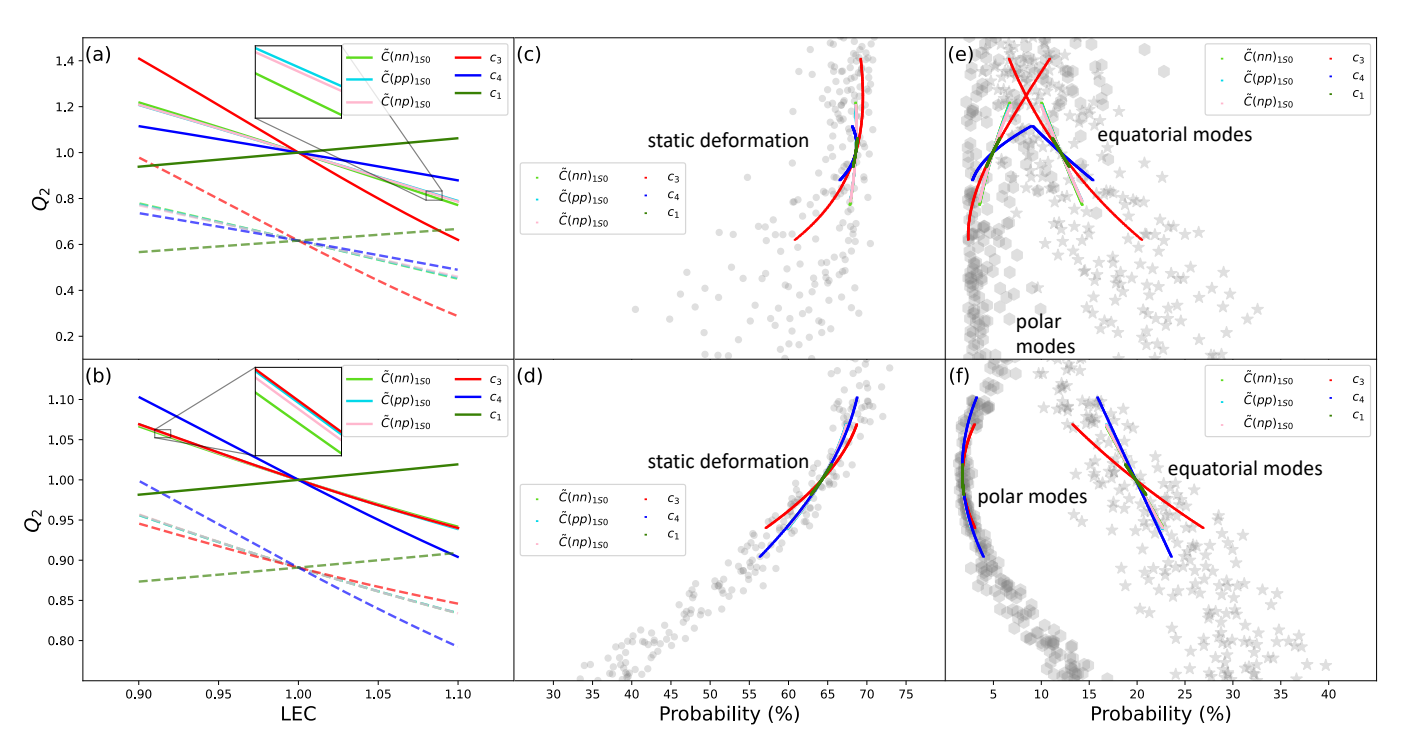


FIG. 10:  $Q_2$  quadrupole moments (solid), relative to their NNLO<sub>opt</sub> values, of (a) the  $^6$ Li  $^{+}_{g.s.}$ , (b)  $^6$ Li  $^{+}_{1}$ , and (c)  $^{12}$ C  $^{+}_{2}$  states vs. each LEC varied  $\pm 10\%$  around its NNLO<sub>opt</sub> value. Also shown is  $Q_2$  of the dominant shape (dashed). The corresponding probability amplitudes of the dominant shapes are shown for (d)-(f) the static (0p-0h) deformation, together with (g)-(i) the surface oscillations along the symmetry axis (labeled "polar") and perpendicular to it (labeled "equatorial").  $Q_2$  moments obtained from 300 simultaneously varied LEC samples are shown in gray for the static deformation (circles), polar (hexagons), and equatorial modes (stars).